Enhanced critical currents by silver sheeting of $YBa_2Cu_3O_{7-\delta}$ thin films

M. Kienzle, J. Albrecht, R. Warthmann, and H. Kronmüller
Max-Planck-Institut für Metallforschung, Heisenbergstrasse 1, D-70569 Stuttgart, Germany

S. Leonhardt
Max-Planck-Institut für Festkörperforschung, Heisenbergstrasse 1, D-70569 Stuttgart, Germany

Ch. Jooss
Institut für Materialphysik, Georg-August-Universität, Windausweg 2, D-37073 Göttingen, Germany

Magneto-optical investigation of flux penetration into high-temperature superconducting thin films allows the determination of the local critical current density j_c by an inversion scheme of Biot-Savart's law. This method is used to examine the influence of silver sheeting on j_c in thin films of $YBa_2Cu_3O_{7-\delta}$ (YBCO) quantitatively. It can be found that a feasible silver covering layer on top of a YBCO thin film can enhance the critical current density by up to 50%. Spatially resolved measurements of the magnetic-flux density distribution in partly silver covered YBCO films show the influence of the cover layer on the current pattern in the superconductor. The measured enhancement of the critical current density, that is induced by the silver layer, has its origin in a spatially varying proximity effect between superconductor and silver layer which leads to a strong variation of the flux-line energies on a small length scale. This variation is directly related to an additional pinning force density on the flux lines. A detailed model is developed that can explain the measured enhancement of the critical current density by considering this additional pinning.

PACS number(s): 74.60.Jg, 74.50.+r, 74.72.Bk, 74.60.Ge

The critical current density is one of the most crucial properties of high-temperature superconductors for both physical understanding and applications. A lot of work has been carried out on the question of how to enhance the critical current density of superconducting material. Very high critical currents can be observed in epitaxially grown thin films of high-temperature superconductors.[1–3] Current densities of up to $j_c \approx 8 \times 10^{11}$ A/m^2 at $T = 5$ K can be found in films of $YBa_2Cu_3O_{7-\delta}$ (YBCO).[4,5] This originates from the high density of different lattice defects that act as effective pinning sites for the flux lines.[4–9] Detailed theoretical descriptions of these pinning scenarios can be found in the reviews of Blatter *et al.*[10] and Brandt.[11] To exploit these high values of j_c for current transport applications it is necessary to contact the superconductors with a common, nonsuperconducting current supply. This is usually done by evaporating thin films of noble metals onto the top of the superconductor which acts as contact pads. Silver layers were especially found to have excellent characteristics for this application.[12] The scope of this paper is the investigation of correlations between silver cover layers and the critical current densities in thin films of high-temperature superconductors.

We present measurements on the influence of silver covering layers on the superconducting characteristics of YBCO thin films. In our experiment YBCO thin films are used which are manufactured by laser deposition on [001] SrTiO$_3$ substrates. An etching process is performed to pattern the samples into long strips with a width of 500 μm and varying thicknesses d_s between 100 and 220 nm. Of each of the YBCO films one-half was covered with silver layers with thicknesses d_n between 30 and 350 nm, which were deposited by a sputtering technique. This geometry allows us to

compare the same YBCO thin film with and without a silver covering layer, excluding all other possible variations that might occur in the case of using different samples.

These samples are placed in a helium cryostate and all measurements are performed at $T = 5$ K after zero-field cooling. After applying an external magnetic field, the flux density distribution in the samples is investigated. The spatially resolved z component of the magnetic-flux density is measured by means of magneto-optics. As a field-sensing layer we use a ferrimagnetic FeGdY-garnet film that exhibits a strong Faraday effect.[13,14] This garnet film is placed onto the sample, and then observed by a polarization-light microscope connected to a charge-coupled device camera. This method yields gray scale images of the light-intensity distribution that is generated by the magnetic-flux density distribution slightly above the YBCO strip with a spatial resolution of approximately 3–5 μm. The limiting factor of the spatial resolution is the thickness of the magneto-optically active layer because the magnetic-flux density pattern is blurred with increasing distance to the surface of the sample. In the obtained images high magnetic-flux densities appear as bright parts, and dark parts refer to a low magnetic-flux density. From the light-intensity data the flux density distribution can be obtained quantitatively by using a nonlinear calibration function which takes the intrinsic properties of the garnet film into account.[15]

Figure 1 shows the measured and calibrated magnetic-flux distribution of a sample that consists of an optimally doped YBCO film with a thickness $d_s = 100$ nm covered on the right part with a 300-nm-thick silver layer. The image is obtained at an applied external field of $\mu_0 H_{ex} = 24$ mT after zero-field cooling. To reduce perturbing polarization effects of the microscope the image of the zero-field cooled state is subtracted.
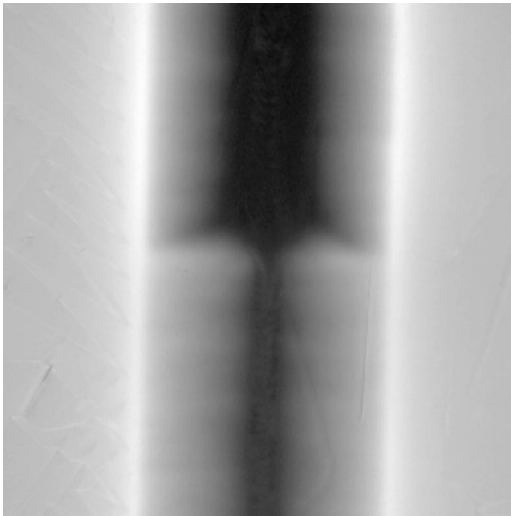
FIG. 1. Gray scale image of the flux density distribution in the superconducting strip measured at $\mu_0 H_{ex} = 24$ mT and $T = 5$ K. The width of the strip is 500 μm.

In the gray scale representation the difference between the silver sheeted and the unmodified part is obvious. The penetration depth of the magnetic-flux density is much smaller for the YBCO-silver double layer. This is related to a significantly enhanced critical current density in this area. The interface between uncovered and covered superconductors shows additional features. The two parts of the strip are separated by a bright line visible in the center of Fig. 1. This line is a so-called d^--discontinuity line, characterized by a jump in the magnitude of the current density.[16] At the crossings of the d^- line with the border of the sample two more discontinuity lines start, namely, two d^+ lines, visible as black lines having the diagonal course into the region with lower penetration depth. These d^+ lines indicate a change of the direction of the current stream lines.

This knowledge is now applied to develop a model for the corresponding current pattern in the superconductor. To reduce geometric difficulties, a strip is assumed with an infinite length and a thickness which is much smaller than the finite width. This sample geometry leads to a quasi-two-dimensional problem. The strip is divided into two areas of different values of the critical current densities j_{c1} and j_{c2}. Under the condition that the Bean assumption $j_c = $ const is valid in each area, it is possible to construct the current pattern geometrically.[17] Note, that the exact solution can only be found for the fully penetrated state. The current pattern for a thin superconducting strip with two different j_c's is depicted in Fig. 2.

The thin black lines are representing the current stream lines; the distance between them gives the magnitude of the current density. The discontinuity lines are shown as thick black lines and their positions are determined by the ratio of the two current densities in the left and in the right parts of the strip. There is a clear correspondence between the discontinuity lines that appear in this simple model and the discontinuity lines observed in Fig. 1.

To perform a useful comparison with the experimental data it is necessary to obtain the corresponding current pat-
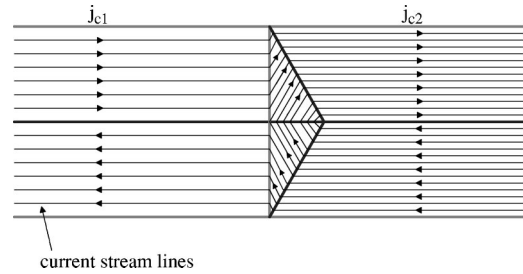
FIG. 2. Sketch of the current-density distribution in a superconducting thin strip with two different critical currents according to Bean's model.

tern to the observed flux density distribution in Fig. 1. This can be achieved by a model-independent, numerical calculation: the relation between the z component of the flux density distribution and the desired current-density distribution is given by the equation of Biot and Savart. Assuming a two-dimensional current distribution, which means there are only currents in the film plane and these currents are constant along the direction perpendicular to the film plane, it is possible to invert Biot-Savart's law in an unambigious way. These assumptions are fulfilled very well for the case of the investigated thin-film geometry. Using div $j = 0$ as a second equation one is able to determine j_x and j_y, the in-plane components of the current density, from the measured B_z data. For a detailed description of the inversion scheme see Jooss *et al.*[18]

A first representation of the current-density distribution calculated from the magnetic-flux pattern in Fig. 1 can be given by plotting the corresponding current stream lines. In Fig. 3 the stream lines overlie the flux density distribution in the superconductor. The magnitude of the current density is proportional to the inverse distance of the stream lines and this magnitude is obviously higher in the right, silver-sheeted area. The background gray scale in Fig. 3 shows some zigzag lines in the center of the sample. These lines are generated by magnetic domain boundaries in the field-sensing layer.
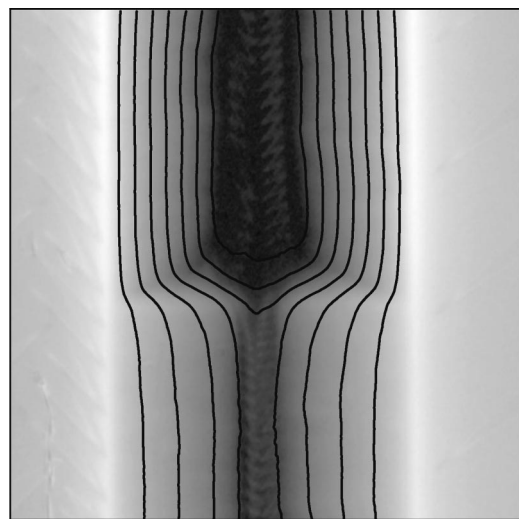
FIG. 3. Overlay of the gray scale image of Fig. 1 and the calculated current stream lines.
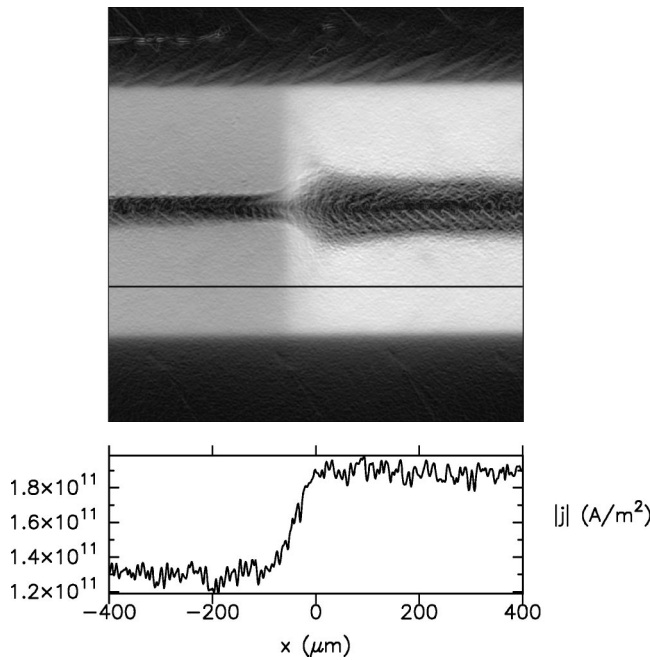
FIG. 4. Gray scale image of the magnitude of the current density corresponding to the stream lines in Fig. 3. The profile below gives the value of the current density along the black line.

In addition to this a lot of features of the current model in Fig. 2 can be recognized. The first we will mention is the continuous but localized bending of the current stream lines at the discontinuity lines that follows the prediction of the model. The finite curvature radii at the d lines are due to the influence of finite electric fields.[19] Another accordance to the model is the retracing of the inner stream lines in the high-current area at the border of the silver sheeting. The three inner stream lines in the right part of the image show the same behavior as the corresponding lines in Fig. 2.

To get a quantitative value of the current enhancement by a silver covering layer, in Fig. 4 a gray scale image of the magnitude of the current density is depicted. Bright areas refer to high current densities and the black color indicates vanishing currents. The profile plotted below the image is taken along the black horizontal line in the lower part of the image.

Figure 4 confirms the splitting of the superconducting strip into two parts with constant critical current densities each. This is shown by the light gray in the right part with the high currents and a darker gray in the left part separated by a sharp border. The zigzag structures in the center of the sample are again created by domain structures in the iron-garnet film. A close look on the profile plotted below yields an enhancement of the current density from 1.3×10^{11} A/m^2 in the unmodified region to 1.9×10^{11} A/m^2 in the silver-sheeted region. This is an increase of about 50%.

In the following, a systematic study of this enhancement of the critical current density as a function of the thicknesses d_s of YBCO and d_n of silver is performed to get a deeper insight in the origin of this effect. A first results shown in Fig. 5. The plot shows the relation between the absolute enhancement of the critical current density Δj_c and the inverse
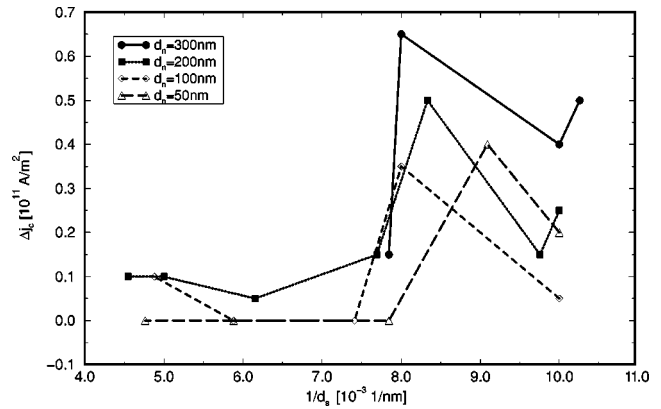
FIG. 5. Enhancement Δj_c of the critical current density in dependence of the thickness d_s of the YBCO film. The different curves refer to different thicknesses d_n of the silver cover layers specified in the top left of the figure.

thickness $1/d_s$ of the superconducting film. The different curves refer to four different thicknesses d_n of the silver covering layer. The curves in Fig. 5 show an increase of the effect for decreasing thicknesses of the superconducting layers. This behavior indicates that the enhancement of j_c by silver sheeting is caused by a surface effect.

Further information can be obtained by investigating the dependence of the effect on the thickness d_n of the normal conducting layer. This scenario is plotted in Fig. 6.

Apart from the sample OA9/1 all measurements show a distict increase of the effect with an increasing thickness d_n of the silver layer. The negligible effect for sample OA9/1 is related to the fact that it is the thickest sample of the series and therefore the least influenced by the surface effect. The data in Fig. 6 prove that the origin of the enhancement of the critical current density is related to the so-called proximity effect. This effect describes the tunneling of Cooper pairs into the nonsuperconducting metal film.[20] It leads to an inhomogeneous extension of the superconducting condensate into the normal conducting metal and thus to a variation of
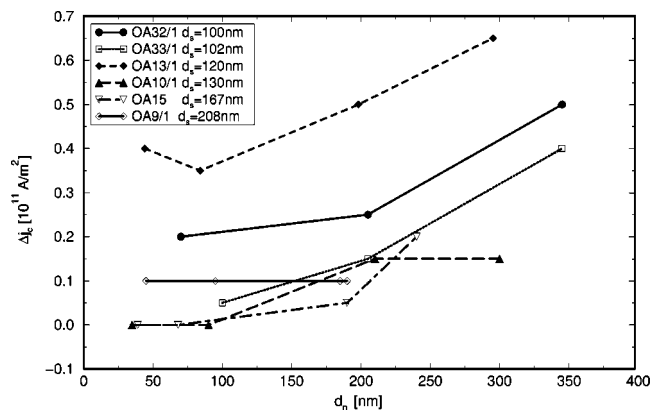
FIG. 6. Enhancement Δj_c of the critical current density in dependence of the thickness d_n of the silver layer. The different curves refer to different thicknesses of the YBCO film which are characterized in the inset in the top left. The "OA" numbers are production codes.

the self-energy of the flux lines. Considering a partly perturbed normal conductor-superconductor interface at the (x,y) plane one gets a spatially varying proximity length $\xi_n(x,y)$. As a result one obtains a spatially varying self-energy E of the flux lines and therefore an additional pinning force.[21] The next section introduces an appropriate model that explains the experimental results based on a description which takes the so-called inhomogeneous proximity effect into account.

Proximity effect means that Cooper pairs penetrate from a superconductor into a noble-metal layer with penetration depths in the range of ~ 100 nm.[20] The transition of the Cooper pairs may be described by a transition probability $\widetilde{W}$ which is related to the microstructure of the superconductor–normal conductor (SN) boundary. It has been shown that the resistivity of the SN boundary which is directly related to the transition probality has to be taken into account to describe the proximity effect properly.[22] Due to precipitates and chemical inhomogeneities including surface roughnesses, this transition probability is modified in space leading to a local variation of the flux-line energy $E(r)$. This leads to a pinning force $f_p=dE_n(r)/dr$, where $E_n(r)$ denotes the energy of vortices extending virtually in the normal conducting silver film. The calculation of $E_n(r)$ is based on the ansatz of Clem[23] for the order parameter Ψ,

$$\Psi(r,z)=f(r)g(z)e^{i\varphi}, \tag{1}$$

where

$$f(r)=\frac{r}{\sqrt{r^2+2\xi_{ab}^2}} \tag{2}$$

describes the radial distribution of $\Psi(r,z)$ and $g(z)$ the dependence of Ψ parallel to the vortex line which is assumed to lie perpendicular to the SN boundary. For $g(z)$ the approximation

$$g(z)=\Psi_0\frac{\widetilde{W}}{\cosh(d_n/\xi_n)}\cosh\left(\frac{z-d_n}{\xi_n}\right), \tag{3}$$

is valid,[24] where Ψ_0 denotes the order parameter in the superconductor and $\widetilde{W}$ describes the jump of the order parameter at the SN boundary. $\widetilde{W}^2$ corresponds to the transmission coefficients of the Cooper pairs at the SN boundary. ξ_n is the proximity length in the normal conductor mentioned above.

For a calculation of the vortex-line energy the circular component A_φ of the vector potential is required, which according to Ref. 23 can approximately be written as

$$A_\varphi(r,z)=\frac{\Phi_0}{2\pi r}\left[1-\frac{R(r)K_1\left(\dfrac{R(r)}{\lambda_n(z)}\right)}{\sqrt{2}\xi_{ab}K_1\left(\dfrac{\sqrt{2}\xi_{ab}}{\lambda_n(z)}\right)}\right] \tag{4}$$

with $R(r)=\sqrt{r^2+2\xi_{ab}^2}$ and the penetration depth in the normal state,

$$\lambda_n=\lambda_L\frac{\cosh(d_n\xi_n)}{\widetilde{W}\cosh\left[\dfrac{1}{\xi_n}(z-d_n)\right]}. \tag{5}$$

The entire energy of the flux line in the normal state now is given by

$$E=\int d^3r\left[\alpha_n(|\Psi|^2-|\Psi_0|^2)\right.$$
$$\left.+\frac{1}{2m*}|(-i\hbar\nabla-2e\mathbf{A})\Psi|^2+\frac{1}{2\mu_0}\mathbf{B}^2\right], \tag{6}$$

where Ψ_0 is the Cooper pair density in the normal conductor for $B=0$. Introducing $\Psi(r,z)$ and $\mathbf{B}=\text{curl }\mathbf{A}$ into Eq. (6) the vortex-line energy can be written as

$$E=\frac{\Phi_0^2\widetilde{W}^2}{4\pi\mu_0\lambda_{ab}^2}F(\xi_n,\kappa,\widetilde{W},d_n), \tag{7}$$

with

$$F(\xi_n,\kappa,\widetilde{W},d_n)=\xi_n\tanh(d_n\xi_n)\left[\frac{5}{8}+\frac{1}{2}\ln(\kappa\widetilde{W})-\frac{\ln 2}{4}\right]$$
$$+\frac{d_n}{\cosh^2(d_n/\xi_n)}$$
$$\times\left[\frac{1}{8}+\frac{1}{2}\ln(\kappa/\widetilde{W})+\frac{d_n}{4\xi_n}-\frac{\ln 2}{4}\right]. \tag{8}$$

κ represents the Ginzburg-Landau parameter and λ_{ab} is the London penetration depth of the superconductor. Details of the calculation can be found in the Appendix.

Under the assumption that the wavelength l of the fluctuations of the transmission probability $|\widetilde{W}|^2$ is larger than λ_{ab} the critical current density due to surface pinning is approximately given by

$$\Delta j_c=\frac{2\Phi_0W_{max}^2}{\mu_0\pi\lambda_L^2l}\times\left[F(\xi_n,\kappa,\widetilde{W}_{max},d_n)\right.$$
$$\left.-\frac{1}{4}\frac{\xi_n}{d_n}\tanh\left(\frac{d_n}{\xi_n}\right)-\frac{1}{4}\frac{d_n}{d_s\cosh^2(d_n/\xi_n)}\right]. \tag{9}$$

where $d\widetilde{W}/dr\approx 4\widetilde{W}_{max}/l$, $\widetilde{W}_{max}$, corresponding to the maximum value of the transmission probability.

Numerical results for Δj_c are presented in Fig. 7 as a function of d_n with ξ_n or $\widetilde{W}_{max}$ as parameters. The superconducting and microstructural parameters used for this calculation are $\kappa=\kappa_{ab}\approx 100$, $\lambda_L=\lambda_{ab}\approx 150$ nm, ξ_n as given in the plots, $\widetilde{W}_m\approx 1/25$,[21] and $l\approx 20$ nm.[15] The numerically determined critical currents Δj_c due to pinning by the inhomogenous proximity effect are of the correct order of magnitude of several 10^{10} A/m^2. Δj_c increases linearly for $d_n<\xi_n$ and approaches a saturation value for $d_n>\xi_n$. The saturation values increase with increasing ξ_n linearly and with increasing $\widetilde{W}_m$ quadratically. A comparison with the experimental re-

(a)

(b)
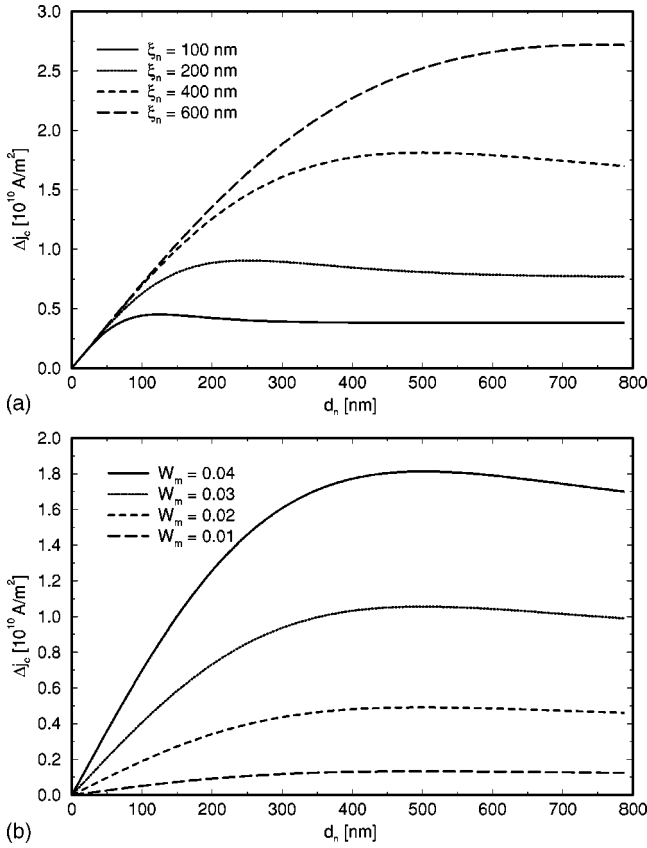
FIG. 7. Top: Δj_c dependent on d_n for different proximity lengths ξ_n ($\widetilde{W}_m = 0.04$, $\Delta x = 20$ nm). Bottom: Δj_c dependent on d_n for different transmission coefficients $\widetilde{W}_m$ ($\xi_n = 400$ nm, $\Delta x = 20$ nm) [Eq. (9)].

sults is shown in Fig. 8, where the experimental quantity $\Delta j_c d_s$ vs d_n is presented. The theoretical curve was obtained for the following parameters: $\widetilde{W}_m = 7.46 \times 10^{-3}$, $l = 27.1$ nm. Furthermore, an additional term, Δj_c^s, has been added to the proximity term which takes care of the microstructural pinning at the degradated surface due to precipitations and plasmaoxidation. The proximity length is estimated from Fig. 8 to be $\xi_n \approx 350$ nm, which is surprisingly large.

In conclusion, we have investigated the influence of a silver covering layer on the critical current of a YBCO thin film. With quantitative analysis of magneto-optical measurements we determined an enhancement of the critical current density of silver-sheeted YBCO of up to 50% compared to the unmodified material. The consideration of YBCO films of varying thicknesses suggests that the effect is caused by a surface mechanism. An additional investigation on silver covering layers between 30 and 300 nm proves the inhomogeneous proximity effect and the related additional pinning force density to be the origin of the enhanced current density. A detailed calculation of the spatial variation of the flux-line energy is able to explain the experimental data properly.
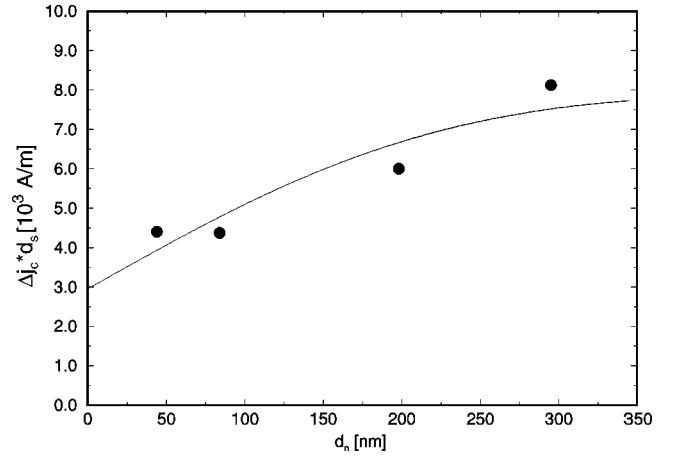
FIG. 8. Comparison of the experimental quantity $\Delta j_c d_s$ with the theoretical prediction [Eq. (9)] as a function of d_n for the specimen of Fig. 3. The fit parameters were $\widetilde{W}_m = 7.46 \times 10^{-3}$, $\Delta x = 27.1$ nm, and $\Delta j_c^s = 0.25 \times 10^{11}$ A/m^2.

APPENDIX: LINE ENERGY

The flux-line energy E_{FL} that is relevant to obtain Eq. (8) is now calculated explicitly. In a normal conducting region E_{FL} is given by

$$E_{FL} = \int_V d^3r \left[\alpha_n(|\Psi|^2 - |\Psi_0|^2) + \frac{1}{2m^*}|(-i\hbar\nabla - 2e\mathbf{A})\Psi|^2 + \frac{\mathbf{B}^2}{2\mu_0} \right]. \quad (A1)$$

$|\Psi_0|^2$ is the charge-carrier density without external magnetic field

$$\Psi_0 = \Psi_B W \cosh\left(\frac{z - d_n}{\xi_n}\right) e^{i\theta}. \quad (A2)$$

$e^{i\theta}$ represents an independent but fixed phase. Note the line energy in the normal conductor is independent of the Landau coefficient β. The line energy can be separated in three parts, the condensation energy, the kinetic energy, and the field energy,

$$E_{FL} = E_\Psi + E_{kin} + E_B. \quad (A3)$$

One obtains

$$E_\Psi = \int_V d^3r \, \alpha_n(|\Psi|^2 - |\Psi_0|^2) \quad (A4)$$

for the condensation part,

$$E_{kin} = \frac{1}{2m^*}\int_V d^3r |(-i\hbar\nabla - 2e\mathbf{A})\Psi|^2 \quad (A5)$$

for the kinetic part, and

$$E_B = \frac{1}{2\mu_0} \int_V d^3 r \mathbf{B}^2 \tag{A6}$$

for the field part. In the following all three parts are considered to be separated from each other.

1. Condensation energy

In a first step the condensation energy shall be calculated:

$$E_\Psi = \int_V d^3 r\, \alpha_n (|\Psi|^2 - |\Psi_0|^2). \tag{A7}$$

The radial part of the order parameter is approximately given by Welch[25] with

$$|f(r)|^2 = 1 - e^{-r^2/\xi_W^2}. \tag{A8}$$

ξ_W is slightly larger than $\sqrt{2}\xi_{ab}$ and gives a value for the flux-line extension. By use of Ψ, Ψ_0, and

$$\alpha_n = \frac{\hbar^2}{2m^* \xi_W^2} \tag{A9}$$

in Eq. (A7), φ and r integration yields

$$E_\Psi = \frac{2\pi\hbar^2 |\Psi_B|^2 W^2}{4m^*} \int_0^{d_n} dz \cosh^2\left(\frac{z-d_n}{\xi_n}\right). \tag{A10}$$

The introduction of λ_n, the penetration depth in the normal state, simplifies Eq. (A10) to

$$E_\Psi = \frac{\phi_0^2}{8\pi\mu_0} \int_0^{d_n} dz\, \frac{1}{\lambda_n^2}. \tag{A11}$$

2. Kinetic energy

The calculation of the kinetic energy starts with the modified Eq. (A5),

$$E_{kin} = \frac{1}{2m^*} \int_V d^3 r [\hbar^2 |\nabla\Psi|^2$$
$$+ 2ie\hbar\mathbf{A}(\Psi^*\nabla\Psi - \Psi\nabla\Psi^*) + 4e^2\mathbf{A}^2 |\Psi|^2]. \tag{A12}$$

With $A_\varphi(r,z)$ and the ansatz for the order parameter,

$$\Psi(r,z) = \Psi_B e^{i\varphi} \frac{r}{\sqrt{r^2 + \xi_\nu^2}} W \cosh\left(\frac{z-d_n}{\xi_n}\right), \tag{A13}$$

writing ξ_ν for $\sqrt{2}\xi_{ab}$ one obtains

$$E_{kin} = \frac{\hbar^2 |\Psi_B|^2}{2m^*} \int_V d^3 r\, W^2 \cosh^2\left(\frac{z-d_n}{\xi_n}\right)$$

$$\times \left[\frac{\xi_\nu^4}{(r^2 + \xi_\nu^2)^3} + \frac{K_1^2\left(\frac{R}{\lambda_n}\right)}{\xi_\nu^2 K_1^2\left(\frac{\xi_\nu}{\lambda_n}\right)} \right]. \tag{A14}$$

φ and r integration together with the recursion formula for the MacDonald functions K_n simplify Eq. (A14) to

$$E_{kin} = \frac{\phi_0^2}{8\pi\mu_0} \int_0^{d_n} dz \left\{ \frac{K_0^2\left(\frac{\xi_\nu}{\lambda_n}\right)}{\lambda_n^2 K_1^2\left(\frac{\xi_\nu}{\lambda_n}\right)} + \frac{2K_0\left(\frac{\xi_\nu}{\lambda_n}\right)}{\xi_\nu\lambda_n K_1\left(\frac{\xi_\nu}{\lambda_n}\right)} - \frac{1}{2\lambda_n^2} \right\}. \tag{A15}$$

3. Field energy

The last contribution is the magnetic-field energy. After φ and r integration one obtains

$$E_B = \frac{\phi_0^2}{8\pi\mu_0} \int_0^{d_n} \frac{1}{\lambda_n^2} \left(1 - \frac{K_0^2\left(\frac{\xi_\nu}{\lambda_n}\right)}{K_1^2\left(\frac{\xi_\nu}{\lambda_n}\right)} \right). \tag{A16}$$

4. z integration

The remaining problem is now the z integration of the sum of all contributions,

$$E_{FL} = \frac{\phi_0^2}{8\pi\mu_0} \int_0^{d_n} dz \left\{ \frac{2K_0\left(\frac{\xi_\nu}{\lambda_n}\right)}{\xi_\nu\lambda_n K_1\left(\frac{\xi_\nu}{\lambda_n}\right)} + \frac{3}{2\lambda_n^2} \right\}. \tag{A17}$$

This is an integral that cannot be solved analytically. Therefore we have to introduce approximations for the MacDonald functions. The quotient ξ_{ab}/λ_{ab} is of the order of 10^{-2} for YBCO and with $W < 10^{-2}$ the arguments of the MacDonald functions are very small. This leads to the first-order terms

$$K_0\left(\frac{\xi_\nu}{\lambda_n}\right) \to \ln\left(\frac{\lambda_n}{\xi_\nu}\right),$$

$$K_1\left(\frac{\xi_\nu}{\lambda_n}\right) \to \frac{\lambda_n}{\xi_\nu}. \tag{A18}$$

Equation (A17) can be substituted by

$$E_{FL} = \frac{\phi_0^2 W^2}{4\pi\mu_0\lambda_B^2} \int_0^{d_n} dz\, \cosh^2\left(\frac{z-d_n}{\xi_n}\right)$$

$$\times \left\{ \frac{3}{4} - \ln\left[\frac{\xi_\nu}{\lambda_B} W \cosh\left(\frac{z-d_n}{\xi_n}\right)\right] \right\}. \tag{A19}$$

using λ_n from Eq. (5).

With partial integration and the substitution $\widetilde{z}=z-d_n/\xi_n$ we can write

$$E_{FL}=\frac{\phi_0^2 W^2}{4\pi\mu_0\lambda_B^2}\left[\frac{\xi_n}{4}\sinh\left(\frac{2d_n}{\xi_n}\right)+\frac{d_n}{2}\right]$$

$$\times\left\{\frac{3}{4}-\ln\left[\frac{\xi_\nu}{\lambda_B}W\cosh\left(\frac{d_n}{\xi_n}\right)\right]\right\}+\frac{\phi_0^2 W^2}{16\pi\mu_0\lambda_B^2}\left[\frac{\xi_n}{2}\sinh\right.$$

$$\left.\times\left(\frac{2d_n}{\xi_n}\right)-d_n\right]+\frac{\phi_0^2 W^2\xi_n}{8\pi\mu_0\lambda_B^2}\int_{-d_n/\xi_n}^{0}d\widetilde{z}\widetilde{z}\tanh(\widetilde{z}).$$

$$(A20)$$

The integral over $\widetilde{z}\tanh(\widetilde{z})$ remains. An approximate solution of the integral can be given by

$$\int_{-d_n/\xi_n}^{0}d\widetilde{z}\widetilde{z}\tanh(\widetilde{z})\approx\frac{1}{2}\left(\frac{d_n}{\xi_n}\right)^2. \qquad (A21)$$

Summing up all results and reintroducing $\widetilde{W}$, the transmission coefficient, $\xi_B\approx\xi_\nu/\sqrt{2}$, the coherence length and $\kappa=\lambda_B/\xi_B$, the Ginzburg-Landau parameter, the line energy of a flux line in a normal conductor perpendicular to a superconductor interface, can be written as

$$E_{FL}=\frac{\phi_0^2\widetilde{W}^2}{4\pi\mu_0\lambda_B^2}\left[\xi_n\tanh\left(\frac{d_n}{\xi_n}\right)\left(\frac{5}{8}-\frac{\ln 2}{4}\right)\right.$$

$$+\frac{d_n}{\cosh^2\left(\frac{d_n}{\xi_n}\right)}\left(\frac{1}{8}-\frac{\ln 2}{4}\right)+\frac{d_n^2}{4\xi_n\cosh^2\left(\frac{d_n}{\xi_n}\right)}$$

$$\left.+\left(\frac{\xi_n}{2}\tanh\left(\frac{d_n}{\xi_n}\right)+\frac{d_n}{2\cosh^2\left(\frac{d_n}{\xi_n}\right)}\right)\ln\left(\frac{\kappa}{\widetilde{W}}\right)\right].$$

$$(A22)$$

[1] Ch. Gerber, D. Anselmetti, J.G. Bednorz, J. Mannhart, and D.G. Schlom, Nature (London) **350**, 279 (1991).

[2] J. Gao, B. Häuser, and H. Rogalla, J. Appl. Phys. **67**, 2512 (1990).

[3] T. Nagaishi, H. Itozaki, S. Tanaka, T. Matsuura, N. Ota, N. Fujimori, and S. Yazu, Jpn. J. Appl. Phys., Part 2 **30**, L718 (1991).

[4] Ch. Jooss, R. Warthmann, H. Kronmüller, T. Haage, H.-U. Habermeier, and J. Zegenhagen, Phys. Rev. Lett. **82**, 632 (1999).

[5] J.M. Huijbregtse, B. Dam, R.C.F. van der Geest, F.C. Klaasen, R. Elberse, J.H. Rector, and R. Griessen, Phys. Rev. B **62**, 1338 (2000).

[6] B. Roas, L. Schultz, and G. Saemann-Ischenko, Phys. Rev. Lett. **64**, 479 (1990).

[7] R. Gross, A. Gupta, E. Olsson, and G. Koren, Appl. Phys. Lett. **57**, 203 (1990).

[8] T.L. Hylton and M.R. Beasley, Phys. Rev. B **41**, 11 669 (1990).

[9] J. Mannhart, D. Anselmetti, J.G. Bednorz, A. Catana, Ch. Gerber, K.A. Müller, and D.G. Schlom, Z. Phys. B: Condens. Matter **86**, 177 (1992).

[10] G. Blatter, M.V. Feigel'man, A.I. Larkin, and V.M. Vinokur, Rev. Mod. Phys. **66**, 1125 (1994).

[11] E.H. Brandt, Rep. Prog. Phys. **58**, 1465 (1995).

[12] S. Jin, M.E. Davis, T.H. Tiefel, R.B. van Dover, R.C. Sherwood, H.M. O'Bryan, G.W. Kammlott, and R.A. Fastnacht, Appl. Phys. Lett. **54**, 2605 (1989).

[13] L.A. Dorosinskii, M.V. Indenbom, V.A. Nikitenko, Yu.A. Ossip'yan, A.A. Polyanskii, and V.K. Vlasko-Vlasov, Physica C **203**, 149 (1992).

[14] M. Yu.Goosev, N.S. Neustroev, M.R. Grechishkin, and S.E. Ilyashenko, J. Magn. Magn. Mater. **157-158**, 305 (1996).

[15] Ch. Jooss, R. Warthmann, A. Forkl, H. Kronmüller, B. Leibold, and H.-U. Habermeier, Physica C **266**, 235 (1996).

[16] Th. Schuster, M.V. Indenbom, M.R. Koblischka, H. Kuhn, and H. Kronmüller, Phys. Rev. B **49**, 3443 (1994).

[17] Th. Schuster, H. Kuhn, E.H. Brandt, M.V. Indenbom, M. Kläser, G. Müller-Vogt, H.-U. Habermeier, H. Kronmüller, and A. Forkl, Phys. Rev. B **52**, 10 375 (1995).

[18] Ch. Jooss, R. Warthmann, A. Forkl, and H. Kronmüller, Physica C **299**, 215 (1998).

[19] A. Gurevich and J. McDonald, Phys. Rev. Lett. **81**, 2546 (1998).

[20] G. Deutscher and P.G. de Gennes, in *Superconductivity*, edited by R. Parks (Marcel Dekker, New York, 1969), Vol. 2.

[21] M.Yu. Kupryanov and K.K. Likharev, Usp. Fiz. Nauk. **160**, 49 (1990) [Sov. Phys. Usp. **33**, 340 (1990)].

[22] C. Ciuhu and A. Lodder, Phys. Rev. B **64**, 224526 (2001).

[23] J.R. Clem, J. Low Temp. Phys. **18**, 427 (1975).

[24] A.A. Golubov and M.Yu. Kupriyanov, Zh. Éksp. Teor. Fiz. **105**, 1442 (1994) [Sov. Phys. JETP **78**, 777 (1994)].

[25] D.O. Welch, IEEE Trans. Magn. **21**, 827 (1985).